Article

A Multistable Discrete Memristor and Its Application to Discrete-Time FitzHugh–Nagumo Model

Mohd Taib Shatnawi [1,*]**, Amina Aicha Khennaoui** [2]**, Adel Ouannas** [3]**, Giuseppe Grassi** [4]**, Antonio V. Radogna** [4]**, Anwar Bataihah** [5] **and Iqbal M. Batiha** [6,7]

1   Department of Basic Science, Al-Huson University College, Al-Balqa Applied University, Irbid 21510, Jordan
2   TLSI Department, NTIC Faculty, University of Constantine 2, Constantine 25000, Algeria
3   Department of Mathematics and Computer Science, University of Larbi Ben M'hidi,
    Oum El Bouaghi 04000, Algeria
4   Dipartimento Ingegneria Innovazione, Universita del Salento, 73100 Lecce, Italy
5   Ministry of Education, Amman 11118, Jordan
6   Department of Mathematics, Faculty of Science and Information Technology, Al Zaytoonah University of
    Jordan, Amman 11733, Jordan
7   Nonlinear Dynamics Research Center (NDRC), Ajman University, Ajman 346, United Arab Emirates
*   Correspondence: taib.shatnawi@bau.edu.jo

Abstract: This paper presents a multistable discrete memristor that is based on the discretization of a continuous-time model. It has been observed that the discrete memristor model is capable of preserving the characteristics of the continuous memristor model. Furthermore, a three-dimensional memristor discrete-time FitzHugh–Nagumo model is constructed by integrating the discrete memristor into a two-dimensional FitzHugh–Nagumo (FN) neuron model. Subsequently, the dynamic behavior of the proposed neuron model is analyzed through Lyapunov exponents, phase portraits, and bifurcation diagrams. The results show multiple kinds of coexisting hidden attractor behaviors generated by this neuron model. The proposed approach is expected to have significant implications for the design of advanced neural networks and other computational systems, with potential applications in various fields, including robotics, control, and optimization.

Keywords: multistable discrete memristor map; FitzHugh–Nagumo model; Lyapunov exponents; phase portraits; bifurcation diagrams

1. Introduction

The memristor is a nonlinear resistor with a memory function, initially established by Leon Chua in 1971 [1]. However, it was only with the recognition of memristor behavior at the nanoscale by Hewlett–Packard engineer Williams in 2008 that it gained significant attention for its potential uses [2,3]. The memristor has been recognized as the fourth fundamental circuit element, alongside resistance, capacitance, and inductance. Due to its exceptional properties of nonlinearity and its characteristics of memory effect, the memristor has been broadly used in many areas, such as image or voice encryption, circuits and nonlinear systems, neural networks, and nonvolatile memory devices, see [4–6], and for further possible applications, see [7–12].

At present, the discrete memristor model is known as a research hotspot. Numerous scholars have dedicated themselves to the analysis of chaotic phenomena in discrete memristors. In [13], Bao et al. introduced into the logistic map a novel discrete memristor map. In [14], the chaotic behavior of a mathematical model of such a memristor was illustrated in detail. In addition and with the window function, a fractional discrete memristor model was explored in [15], while in [16], Khennaoui et al. presented a 2D fractional memristor map with the use of the Grunwald–Letnikov definition. Li et al. [17] applied offset boosting and amplitude control to a discrete memristive chaotic map. Recently, hidden

attractors have also been discovered in some discrete memristor-based maps [18]. Based on the Lozi map, Wang and his co-authors included a discrete-time memristor to create a memristive Lozi map [19]. Their generated map exhibited hidden dynamics evolutions with a multistability property as well. While memristors have gained significant traction in continuous-time-domain chaotic systems, there remains substantial untapped potential for the exploration and creation of discrete memristive chaotic maps. Moreover, discrete memristors exhibit enhanced suitability for integration into discrete-time-domain chaotic maps and digital circuits, thereby paving the way for their broader application. Thus, the future lies in the development of advanced discrete memristive system models, representing a pivotal pathway towards unlocking the full capabilities of memristor technology.

There have been various neuron maps developed to study the firing patterns of neurons, including the Hodgkin–Huxley (HH) model [20], the Morris–Lecar model [21], the Chay model [22], and the FitzHugh–Nagumo (FHN) model [23], see also [24–26]. The FHN neuron model was derived as a simplified version of the Hodgkin–Huxley neuron model, known for its efficacy in theoretical analysis and numerical simulation of neuron electrical activities. Synapses play a vital role in facilitating functional connections and information transmission between neurons. Among them, autapses stand out as a unique synaptic structure formed by the connection between a neuron's axons and its own dendrites. Memristor devices offer a promising application as synapses in neuromorphic systems. In [27], the authors investigated a model of the FitzHugh–Nagumo neuron with memristive autapse. Their study revealed that the proposed model was able to exhibit extreme multistability. The multistable dynamics of an autonomous Morris– Lecar neuron have been addressed in [28]. Furthermore, [29,30] investigated the collective dynamic behaviors of multiple neurons coupled through memristor-based autapses.

Discretization serves the purpose of simplifying mathematical models, enhancing computer processing, and promoting stable processing results. However, it remains unclear whether discrete systems can accurately reproduce the dynamic behavior of neurons. Currently, there is limited discussion on the application of discrete memristors in the field of neurons. In reference [31], the authors considered a discretized version of the Izhikevich neuron model and found that the electromagnetic flux can act as an order parameter in the sense that it can tune different firing patterns under the variation of the electromagnetic flux. Hussain et al. [32] investigated the dynamics of a network of multi-weighted FitzHugh–Nagumo neurons, taking into account the effect of electrical, chemical, and ephaptic couplings. In [33], the authors investigated a (2D) discrete Hindmarsh–Rose neuron model based on a novel discrete memristor. They found that the chaotic region became wider when a discrete memristor was introduced. However, for the discrete memristive neuron models, there are relatively few studies on mode transitions and coexisting firing patterns.

Considering this, in this paper, based on a multistable discrete memristor, a discrete generalized FHN neuron model with memristive autapse is presented. The main contributions of this study are summarized as follows: (1) We construct a novel discrete generic memristor model with a multistability property based on a continuous memristor model and analyze its special characteristics. Under various initial states, multiple coexisting pinched hysteresis loops can be exhibited by way of a multistable memristor. This particular memristor is considered more appropriate for creating memristive multistable systems than other discrete memristors because of its initial condition and multistability. The multistability characteristic of the locally active memristor [34] makes it a good way to study the firing behavior of neurons. (2) A three dimensional discrete-time FHN neuron model with memristor autapse is presented through interposing the generic discrete memristor into a 2D generalized discrete-time FN neuron model. It is found that more complex dynamical behavior is generated. Furthermore, the coexisting attractor's behavior might be also discovered in this memristive FN map, signifying the emergence of the dynamics' bistability. This, actually, can be seen in certain neuron maps. Nevertheless, the coexisting asymmetric attractors' phenomenon has not been declared for the FHN neuron map previously. This enables the discrete memristive FHN map to generate further rich dynamics. The phe-

nomenon of coexisting multiple attractors is explored with the help of a set of mathematical tools including the Lyapunov spectrum, phase portraits, and bifurcation diagrams.

2. Analysis of a Novel Discrete Memristor Map

This section is split into two subsections, where the first establishes the discrete memristor map, and the second discusses the pinched hysteresis loops, which are deemed to be an important feature to recognize memristors, for the proposed discrete memeristor map.

2.1. Discrete Memristor Model

Consider a voltage-controlled generic memristor in the continuous-time domain

$$\begin{cases} i(t) = G(x)v(t), \\ \frac{dx}{dt} = g(x, v), \end{cases} \tag{1}$$

where i is the current, v is the voltage, $G(x)$ is the memductance, and x is the memristor state. In [35], Lin et al. established a novel continuous memristor model that can be described as:

$$\begin{cases} i(t) = x(t)v(t), \\ \frac{dx}{dt} = a\sin(x(t)) + bv(t), \end{cases} \tag{2}$$

where a and b denote the memristive parameters. Then, the memristor model (2) can be discretized by introducing the difference theory [13], as

$$\begin{cases} i_n = G(x_n)v_n, \\ \Delta x_n = h[a\sin(x_n) + bv_n], \end{cases} \tag{3}$$

where v_n, i_n, and x_n are the sampling values of $i(t)$, $v(t)$, and $x(t)$ at the n-th iteration respectively. From the forward difference operator $\Delta x_n = x(n+1) - x(n)$, n = 0,1,…, we can deduce

$$\begin{cases} x_1 - x_0 = h[a\sin(x_0) + bv_0], \\ x_2 - x_1 = h[a\sin(x_1) + bv_1], \\ x_3 - x_2 = h[a\sin(x_2) + bv_2], \\ \quad\vdots \quad\quad \vdots \quad\quad \vdots \quad\quad \vdots \\ x_n - x_{n-1} = h[a\sin(x_1) + bv_1]. \end{cases} \tag{4}$$

Summing both sides, we obtain

$$x_{n+1} = x_0 + h\sum_{j=0}^{n}\left[a\sin(x_j) + bv_j\right], \tag{5}$$

where q_0 is the initial state. Equation (8) shows that the current state is associated with all the past states. So, the discrete map has a special memory effect. The noteworthy features of the established memristive mathematical map, comprising amplitude-dependent and frequency-dependent pinched hysteresis loops, are confirmed by means of several numerical results in the upcoming subsections, where the normalized parameters of the nonlinear $G(x)$ are selected as $a = 0.005$, $b = -2$, and $h = 0.001$.

2.2. Pinched Hysteresis Loops

The pinched hysteresis loops are considered as the feature fingerprint to recognize memristors [36]. For the purpose of verifying this excellent characteristic of the established discrete memeristor, we took a discrete sinusoidal voltage $v(n) = A\sin(2\pi f t_n)$ with frequency f and amplitude A. Once $A = 2$ was held, and f was set to $f = 3, 10, 100$, respectively, the $v - i$ curves were graphed as shown in Figure 1. Eight shaped pinched hysteresis loops at the origin according to various excited frequencies are clearly illustrated

in Figure 1a. As the input frequencies increased from 3 to 100, the pinched hysteresis loop decreased step by step and shrank into a single-valued function. When the frequency was kept at $f = 2$, and A was taken as 1, 1.5, 2, respectively, the $v - i$ curves were graphed, as shown in Figure 1b, which describes that the pinched hysteresis was obtained regardless of the stimulus amplitude. The numerical findings given in Figure 1a and Figure 1b demonstrate perfectly that the discrete memristor can behave like memristors in the continuous-time domain.
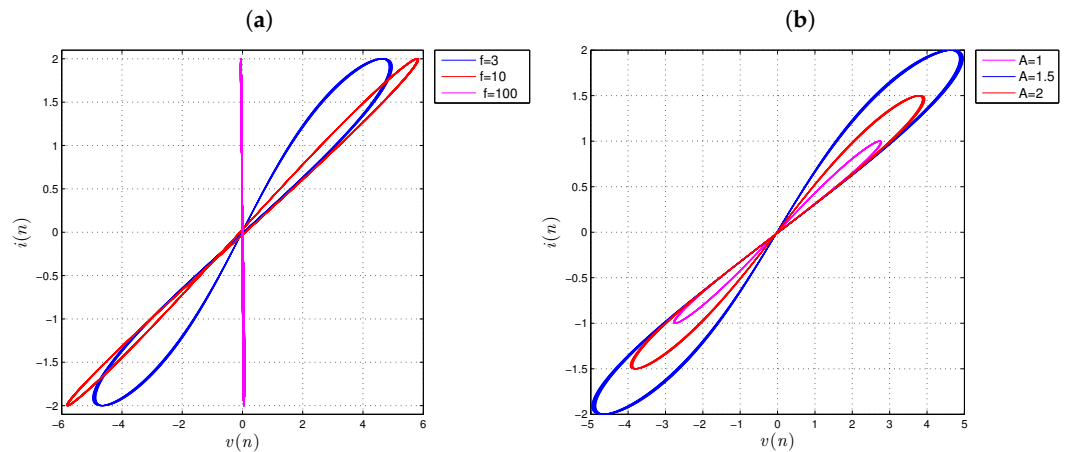

Figure 1. (**a**) Frequency-dependent pinched hysteresis loops of the discrete memristor with $A = 2$. (**b**) Amplitude-dependent pinched hysteresis loops of the discrete memristor with $f = 2$.

Moreover, a memristor that contains n distinct pinched hysteresis loops according to various initial values is named a multistable memristor [37]. To explore the impact of the initial condition on the properties of the discrete memristor, we took the parameters $h = 0.001$, $a = 0.005$, and $b = -2$, with $A = 2$ and $f = 2$, according to various initial conditions $x_0 = -5\pi, -3\pi, 0, 3\pi, 5\pi, 7\pi$. Based on Figure 2, it is found that the discrete memristor exhibited the coexisting pinched hysteresis loops according to the various initial states. Hence, the discrete generic memristor model is multistable. The variation in the initial condition causes the variation in the locally active feature, which could yield rich dynamics when the discrete map is linked with the discrete memristor [38].

In the same regard, a power-off plot (POP) was applied to reveal the nonvolatile characteristics of the discrete memristor [39]. The POP exhibits the dynamic routes of change Δx_n versus state-variable x_n by fixing the input voltage to zero. It must be recognized that each intersection of POP with the x-axis is an equilibrium point; those with a negative slope are stable, and the others are unstable. Hence, when $v = 0$, the discrete memristor state Equation (3) becomes:

$$x_{n+1} - x_n = g(x, 0) = \sin(x). \tag{6}$$

Based on Equation (6), we plotted the POP curve displayed in Figure 3. It has become evident that when $\Delta x_n = 0$, there exist infinitely many intersections positioned at $x = k\pi \, (k \in Z)$, in which, when $k = 2i + 1$, where $i \in Z$, the slopes at x_e are negative, and x_e are stable equilibrium points, and when $k = 2i + 2$, x_e are unstable equilibrium points. Hence, the discrete memristor is nonvolatile [40].
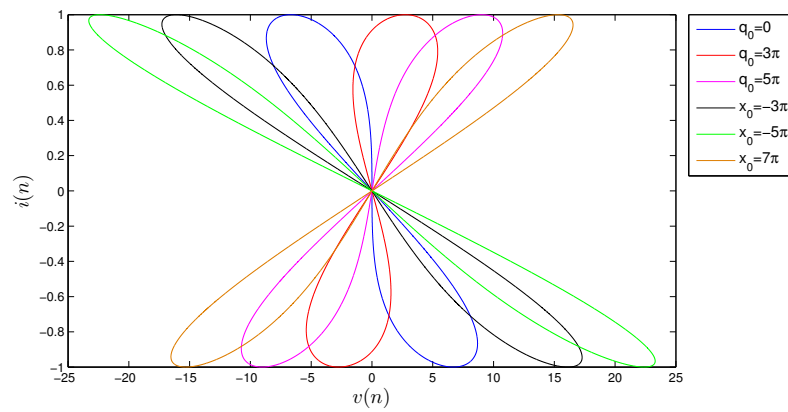
Figure 2. Coexisting pinched hysteresis loops when frequency $f = 0.0009$ and amplitude $A = 1$: with $h = 0.002$.
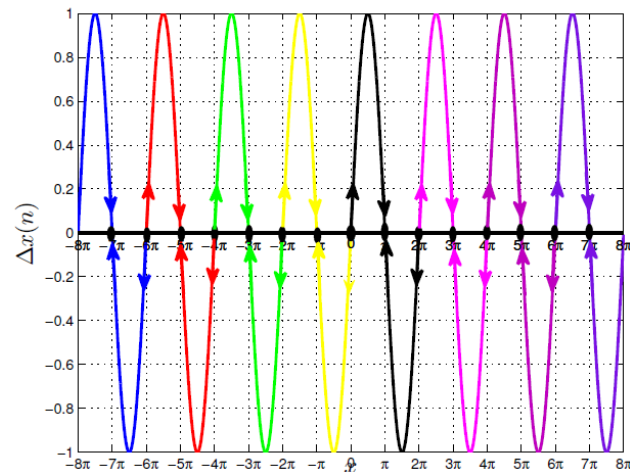

Figure 3. POP of the discrete memristor system (2).

To ensure the accuracy of the discrete solution, an error analysis was conducted to compare the continuous memristor model and the discrete memristor model.

2.3. The Error Analysis

The main difference between the continuous-time memristor model and the discrete memristor model lies in the expression of the charge $x(t)$. The solution of the state Equation (2) can be calculated by

$$x(t) = \int_{-\infty}^{t} (a\sin(x(s)) + bv(s))\mathrm{d}s. \tag{7}$$

For the discrete memristor model:

$$x_{n+1} = x_0 + h\sum_{j=0}^{n}[a\sin(x_1) + bv_1]. \tag{8}$$

Consider the discrete sinusoidal voltage $v = A\sin(2\pi f t)$. Here, we set $e(t) = x(t) - x(t_n)$, $A = 2, x_0 = 0.1, a = 0.005, b = -2$, and $h = 0.001$. The continuous $x(t)$, discrete $x(t_n)$, and error $e(t)$ were, respectively, compared for two different values of $f = 2$ and $f = 5$, and the images are shown in Figure 4a and Figure 4b, respectively. The results show that $x(t)$ and $x(t_n)$ almost coincided. The error $e(t)$ was almost zero. It can be seen from Figure 4 that although the continuous and discrete $x(t)$ were different in form, when the same

parameters were taken, the curves of $x(t)$ and $x(t_n)$ almost coincided, and the error curve was almost zero.
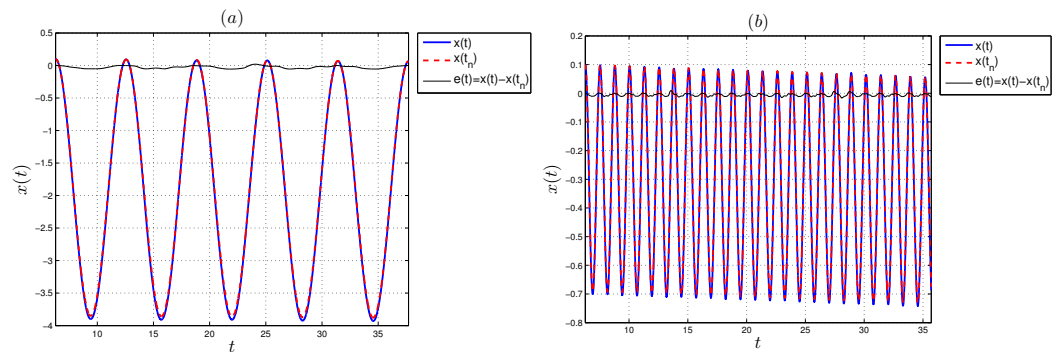

Figure 4. Continuous and discrete $x - t$ and error $e(t)$: (**a**) for frequency $f = 1$ and (**b**) for frequency $f = 5$.

3. A Novel Memristive Neuron Model and Its Dynamical Behaviors

In this section, we describe a generalized version of the discrete-time FHN model, construct a proper memristive discrete FHN neuron model, and then perform the Lyapunov exponents and bifurcation analysis regarding these models, followed by discussion of the memristor initial-value-dependent bifurcation plots.

3.1. Description of a Generalized Discrete-Time FN Model

In 1926, Van der Pol [39] introduced a basic model derived from the nonlinear relaxation oscillator. Additionally, FitzHugh and Nagumo et al. [23] presented the mathematical formulation of excitable neurons, which is expressed through the following dynamical equations:

$$\begin{cases} \frac{dx}{dt} = x - \frac{x^3}{3} - y + I_{ext} + I_{syn}, \\ \frac{dy}{dt} = \varepsilon(x + a - by), \end{cases} \tag{9}$$

where x is the neuron membrane potential, y denotes the recovery variable related to the conductivity of the ion channels, and I_{ext} is the external excitation. The nonlinear therm I_{syn} denotes the autapse current.

The discrete map is acquired from the 2D FHN neuron model (9) with the use of the forward Euler method. In other words, the discrete-time FHN neuron model might be constructed by the following:

$$\begin{cases} x(n+1) = (1+T)x(n) + T\left(-\frac{x^3(n)}{3} - y(n) + I_{ext} + I_{syn}\right), \\ y(n+1) = y(n) + T\varepsilon(x(n) + a - by(n)), \end{cases} \tag{10}$$

where T is the step size, such that $0 < T \le 1$. In the following, we consider the generalized map model, which is obtained from the discrete Equation (10). We analyze the generalized model in the discrete sense but not a truly discrete map. To generalize the discrete FN neuron model, we set $\alpha = 1 + T$, $\beta = T$, $\gamma = 1 - \varepsilon Tb$, $\theta = T\varepsilon$, and $\delta = \varepsilon Ta$ to obtain:

$$\begin{cases} x(n+1) = \alpha x(n) + \beta\left(-\frac{x^3(n)}{3} - y(n) + I_{ext} + I_{syn}\right), \\ y(n+1) = \gamma y(n) + \theta x(n) + \delta. \end{cases} \tag{11}$$

The generalized map is not restricted by the determination of the parameters of the initial discrete map. In other words, the initial map is a particular situation of the generalized map (11).

3.2. Constructed Memristive Discrete FHN Neuron Model

A discrete FHN neuron model with memristive autapse is proposed on the basis of the abovementioned discrete memristor. Its mathematical expression can be written as:

$$\begin{cases} x(n+1) = x(n) - \frac{x^3(n)}{3} - y(n) + I_{ext} + k_1 z(n)x(n), \\ y(n+1) = \gamma y(n) + \theta x(n) + \delta, \\ z(n+1) = z(n) + \sin(z(n)) - k_2 x(n), \end{cases} \tag{12}$$

where k_1 and k_2 are positive, and the system parameters α and β are fixed as $\alpha = 1$ and $\beta = 1$. It is necessary to note that the positive external input current is fixed to $I = 2$.

The equilibrium points of the discrete FHN neuron model with memristive autapse (12) can be generated by considering the following states:

$$\begin{cases} x = x - \frac{x^3}{3} - y + I_{ext} + k_1 zx, \\ y = \gamma y + \theta x + \delta, \\ z = z + \sin(z) - k_2 x. \end{cases} \tag{13}$$

The fixed point is $E = \left(x, \frac{1}{1-\gamma}(\theta x + \delta), \arcsin(x) + 2k\pi \right)$, where $|x| < \frac{1}{k_2}$ can be calculated by the following formula:

$$\begin{cases} F_1(x) = -\frac{x^3}{3} - \frac{\theta}{\gamma-1}x + \left(2 - \frac{\delta}{\gamma-1}\right) + k_1 x \arcsin(k_2 x), \\ F_2(x) = x. \end{cases} \tag{14}$$

Herein, we took the parameters of the system as $\gamma = -0.2$, $\delta = 0.08$, $\theta = 0.108$, $k_1 = -0.06$, and $k_2 = 0.2$. The two functions $F_1(x)$ and $F_2(x)$ are drawn numerically in Figure 5a by the blue and red colors, respectively. The solution to x was determined by calculating the intersection of the two functions F_1 and F_2. As shown in Figure 5a, there was always one intersection between the two functions F_1 and F_2. Therefore, the neuron model addressed in this work possesses an equilibrium point, infinitely. Figure 5b shows the phase diagram of the coresponding chaotic attractor in the 3D plan. Furthermore, our analysis incorporated the Hénon attractor, resulting in the emergence of a Hénon-like map.
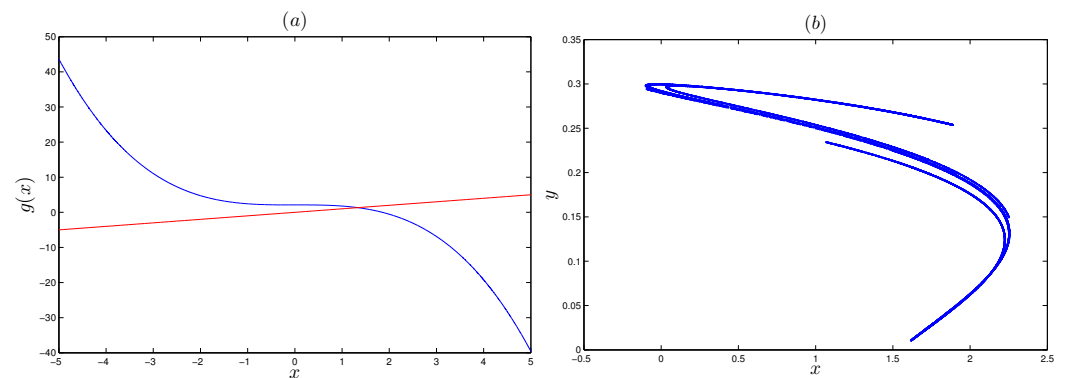

Figure 5. (**a**) Two function curves and their intersections for $k_1 = -0.06$. (**b**) The chaotic attractor emerged from the initial value $(x_0, y_0, z_0) = (0.01, 0.02, 0.1)$ and the system parameters $\gamma = -0.2$, $\delta = 0.08$, $\theta = 0.108$, and $k_1 = -0.06$.

3.3. Lyapunov Exponents and Bifurcation Analysis

With the aim of understanding the dynamics of the discrete FHN neuron model with memristive autapse (12), the two parameters θ and k_1 were deemed as bifurcation parameters, and the bifurcation diagrams were then generated. Initially, we put forward θ as the parameter of bifurcation, and the parameters system's were chosen as $\gamma = -0.2$, $\theta = 0.08$, and $k_2 = 0.2$, with the initial conditions $(x_0, y_0, z_0) = (0.01, 0.02, 0.1)$. Accordingly,

the Lyapunov exponents and bifurcation diagram versus θ for $k_1 = -0.06$, $k_1 = -0.14$, and $k_1 = 0.02$ were generated in Figure 6a, Figure 6b, and Figure 6c, respectively. It is observed that the discrete FHN neuron map with memristive autapse (12) can produce complex dynamical behavior according to various values of bifurcation parameters, where the reverse period doubling bifurcation, the period doubling bifurcation, chaos crisis, and the tangent bifurcation are incorporated. For $k_1 = -0.06$, when the parameter of bifurcation θ was raised in $[-0.1, 0.50]$, it is noticeable, based on the diagram of bifurcation shown in Figure 6a, that the discrete FHN neuron model (12) started from chaos and moved into periodic states via the reverse period doubling route, with some narrow periodic windows at $k_1 = 0.081$. When the system parameter θ was adjusted in $[-0.1, 0.5]$ and $k_1 = -0.14$, the diagrams of bifurcation of the state x_n and the maximum Lyapunov exponents were simulated numerically, as shown in Figure 6b. These diagrams revealed that the discrete FHN neuron model (12) was in a chaotic state at the beginning with a periodic state. When $\theta \in [-0.026, 0.026] \cup [0.032, 0.054]$ the discrete FHN neuron model (12) was in a chaotic state with one positive Lyapunov exponent and eventually moved into a periodic state via the reverse period doubling bifurcation.

Different memristor initial conditions z_0 can produce different types of attractors. When the control parameter was set to $k_1 = 0.02$, the coexistence of attractors of the system was analyzed by the maximum Lyapunov exponents (MLE) and the corresponding bifurcation diagram. The coexisting bifurcation diagram of the state $x(n)$ under $z_0 = 0.1$ (blue diagram) and $z_0 = 4$ (red diagram) was numerically simulated, as shown in Figure 6c. Figure 6d displays the MLE corresponding to the initial condition $z_0 = 4$. At this time, it can be preliminarily judged that the system had coexisting attractors. Under different initial state values, the 3D fractional discrete memristor neuron model produced complex dynamical behavior, where chaos, period, and boundary crises were included.
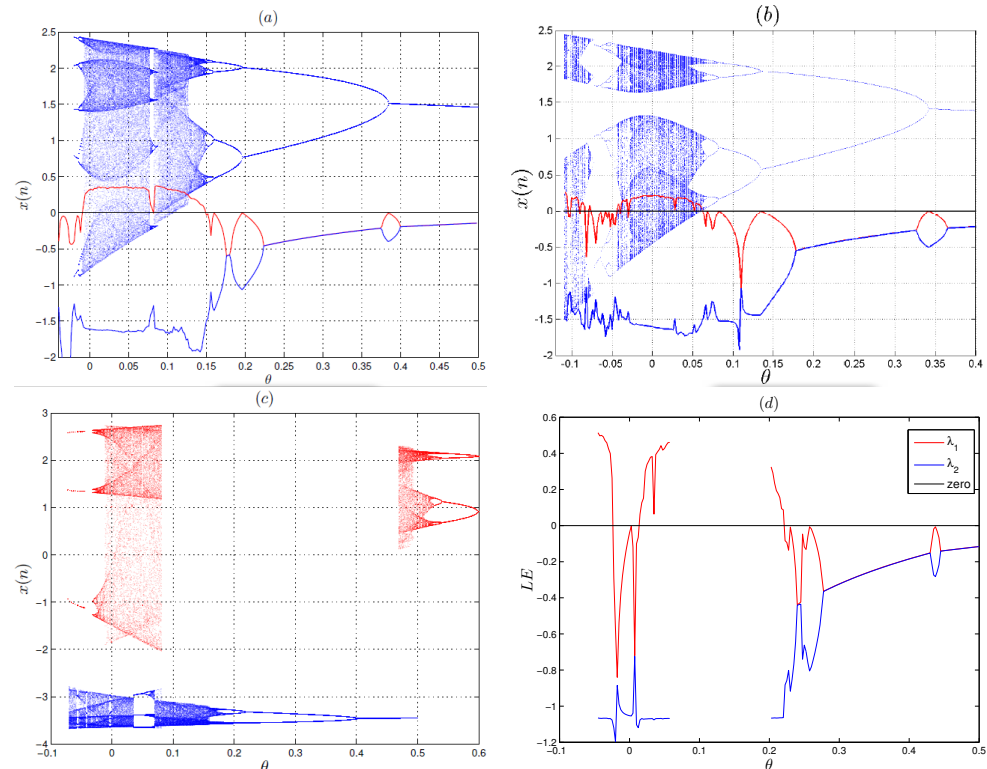

Figure 6. The bifurcation diagram and Lyapunov exponents versus θ for (**a**) $k_1 = -0.06$ and (**b**) $k_1 = 0.14$. (**c**) Coexisting bifurcation for $k_1 = 0.02$ and IC $(0.01, 0.02, 4)$ (red diagram) and $(0.01, 0.02, 0.1)$, $k_1 = 0.02$. (**d**) Lyapunov exponents corresponding to the bifurcation diagram for the initial condition $(0.01, 0.02, 4)$.

Without loss of generality, the phase portraits at several critical values corresponding to Figure 6 are shown in Figure 7. Thus, the phase diagrams display a type of complex behavior, which is consistent with the dynamics, as demonstrated in Figure 6.
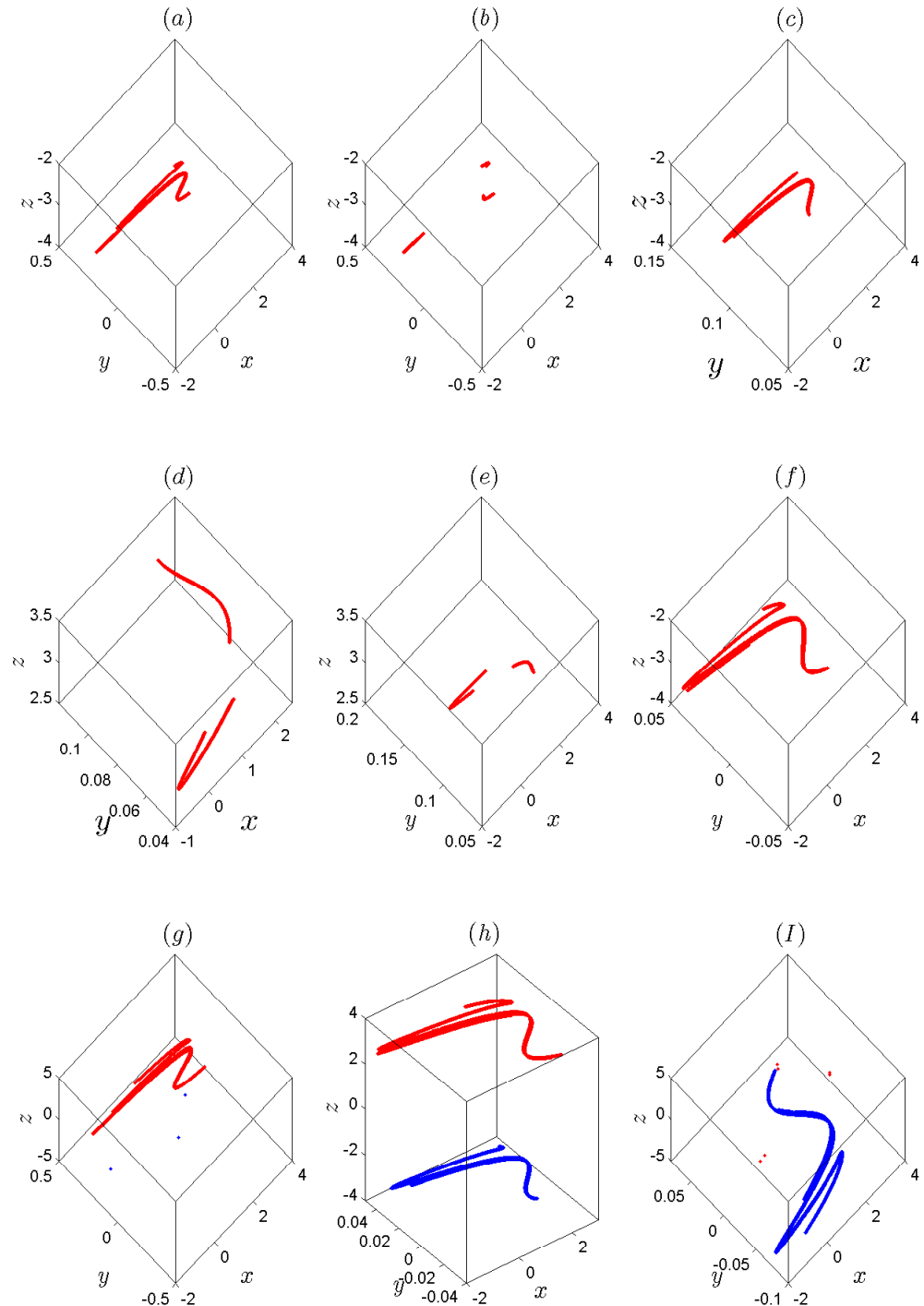

Figure 7. Different strange attractors of the discrete FHN neuron model with memristive autapse (12) for $\gamma = -0.2$, $\theta = 0.08$, and $k_2 = 0.2$ and different system parameters θ and k_1: chaotic attractors: (**a**) $\theta = 0.008$, $k_1 = -0.05$. (**b**) $\theta = 0.066$, $k_1 = -0.05$. (**c**) $\theta = 0.117$, $k_1 = -0.05$. (**d**) $\theta = -0.03$, $k_1 = 0.14$. (**e**) $\theta = 0.004$, $k_1 = -0.14$. (**f**) $\theta = 0.039$, $k_1 = -0.14$. (**g**) Coexisting periodic and chaotic attractor attractor $\theta = 0.045$, $k_1 = 0.02$. (**h**) Coexisting chaotic attractor $\theta = 0.016$, $k_1 = 0.02$. (**i**) Coexisting periodic and chaotic attractors $\theta = -0.026$, $k_1 = 0.02$.

3.4. Memristor Initial-Value-Dependent Bifurcation Plots

Multistability behavior is the coexisting phenomenon of many different kinds of disconnected attractors in a nonlinear dynamical system for a fixed set of system parameters but different initial values, which is a widespread physical phenomena [41].

In this section, bifurcation diagrams and phase portraits are used to explore the remarkable phenomenon of the coexistence of three or more dynamical states under different initial states. Under different initial state values, the discrete memristor FHN neuron model can show several kinds of coexisting multiple attractor behaviors in some neighborhoods of parameter k_1. System parameter k_1 is adjusted in the region $[-0.2, 0]$, the initial values of the neuron model x_0 and y_0 are set as $x_0 = 0.01$ and $y_0 = 0.02$, respectively, the memristor initial value z_0 is selected, respectively, as $z_0 = 0.1, z_0 = 4, z_0 = -8$, and $z_0 = -13$, and the discrete memristor neuron parameters are fixed as $\gamma = -0.2, \theta = 0.108, \delta = 0.081$, and $k_2 = 0.2$. Accordingly, four kinds of bifurcation diagrams in the $y - k_1$ and $z - k_1$ planes are depicted in Figure 8a and Figure 8b, respectively, with different color regions. Obviously, we can find that the discrete memristor FHN neuron model can exhibit four states of coexisting attractors, including coexisting periodic attractors and coexisting chaotic attractors. Figure 8 shows that changing the initial state significantly changes the size and state of the bifurcation diagram under the same parameters. Basically, when the initial condition was assigned to $z_0 = 0.1$, the discrete FHN neuron model (12) changed from a periodic state to a chaotic state via the period doubling bifurcation route, Furthermore, it is found that the bifurcation behaviors were similar to the rest of the initial values $z_0 = 4, z_0 = -8$, and $z_0 = -13$. In addition, it can be observed that the chaotic intervals corresponding to the initial values were obviously different. For instance, when $z_0 = 0.1$, the chaotic interval was located in $[-0.0968, -0.0275]$. However, when the initial state was changed to 4, the hidden chaotic interval was located at $[-0.0332, -0.0098]$.
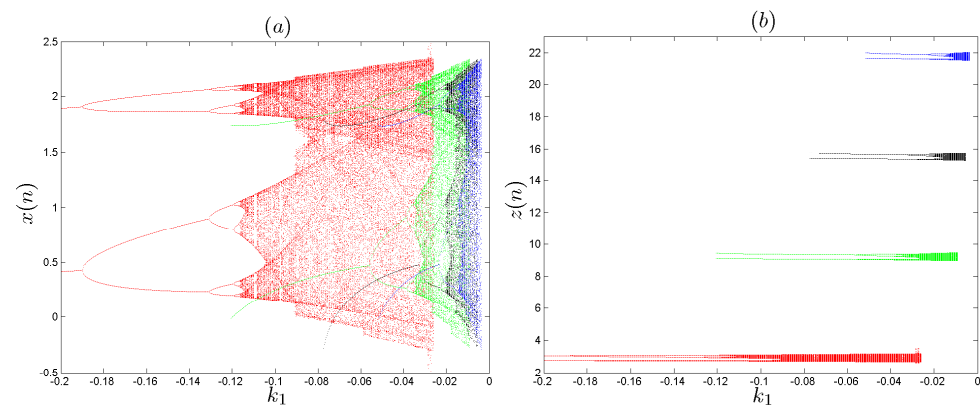

Figure 8. The dynamical systems characterization: (**a**) bifurcation diagrams in the $y - k_1$ plane; (**b**) bifurcation diagrams in the $z - k_1$ plane.

More details of the phenomena of multistability are provided in the following bifurcation analysis. For the initial values (x_0, y_0, z_0) of the discrete FHN model, the memristor initial value z_0 is denoted as the bifurcation parameter, adjusted in the region $[0, 40]$. When the bifurcation parameters $\theta = 0.108$ and $k_1 = -0.01$, the bifurcation plots in the $y - z_0$ and $z - z_0$, are shown in Figure 9a and Figure 9b, respectively. It further illustrates that the discrete FHN has initial value sensitivity and produces complex multistability phenomena. Firstly, Figure 9a shows that the discrete model state changes as z_0 increases. Moreover, Figure 9b shows that with the increase in the memristor initial value z_0, the chaotic attractor preserves a step change in the dynamic amplitude from one level to another level. To show the remarkable phenomena of the multistability of attractors, the phase plots in the $y - z$ plane are depicted in Figure 10, where we selected the five initial values $z_0 = 10, 15, 20, 25$. Thus, the numerical results imply the existence of multistability and demonstrate that the bifurcation routes are closely associated with the third neuron initial conditions.
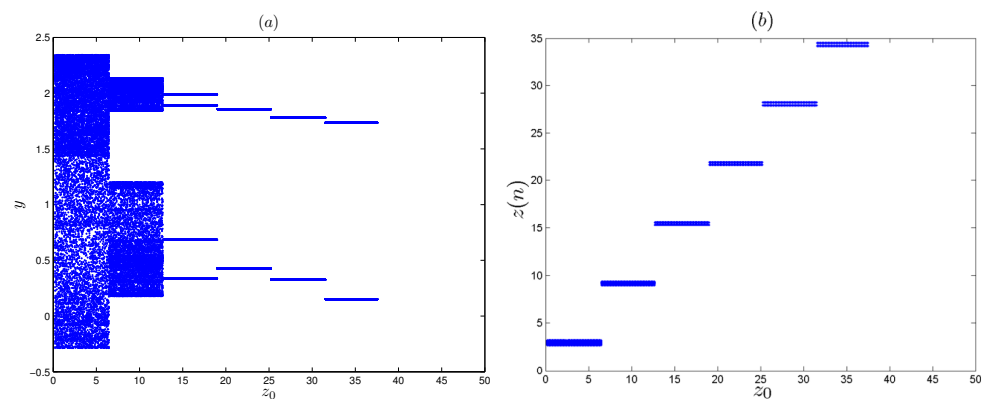
Figure 9. Bifurcation diagrams of the discrete FHN model (12) with initial condition z_0: (**a**) in the 2D plane $y_{max} - z_0$ and (**b**) in the 2D plane $z_{max} - z_0$.
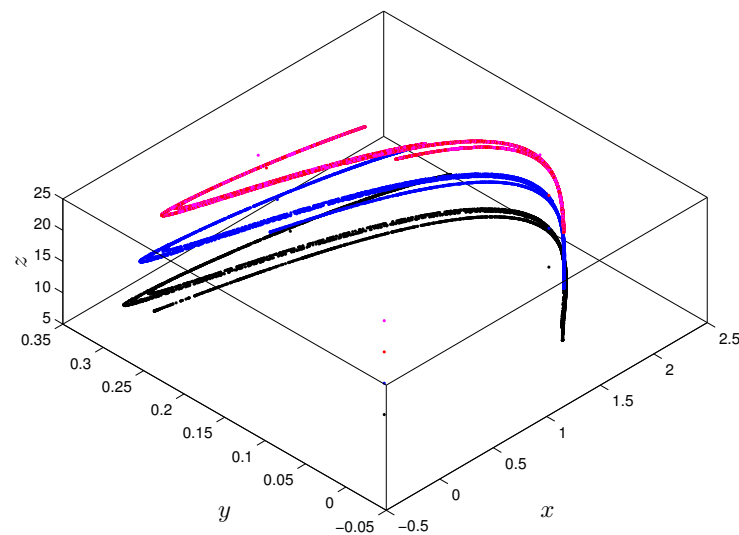

Figure 10. Coexisting multiple attractors for different initial values of z_0 and for $x_0 = 0.01$ and y(1) = 0.02.

4. Conclusions

In this work, based on a multistable discrete memristor, the discrete generalized FHN neuron model with memristive autapse was proposed. The proposed neuron model was then investigated in view of studying the resultant Lyapunov exponents, phase portraits, and bifurcation diagrams. This produced, with the help of different initial values, a remarkable phenomenon of the coexistence of an infinite number of attractors. Although some memristive neuron models and their chaotic dynamics were investigated, it is still in the infant stage and many need to be further explored. We believe that investigating the chaotic dynamics of discrete memristive neuron models will help to elucidate more detailed functions of the brain as well as engineering applications. Based on these, it is believed that this study may contribute to the theoretical research of discrete memristor. In the near future, we will try to apply it to synchronization control, image encryption, and a random number generator.

References

1. Chua, L.O. Memristor-The missing circuit element. *IEEE Trans. Circuit Theory* **1971**, *18*, 507–519. [CrossRef]
2. Strukov, D.B. The missing memristor found. *Nature* **2008**, *453*, 80. [CrossRef] [PubMed]
3. Bezziou, M.; Dahmani, Z.; Jebril, I.; Belhamiti, M.M. Solvability for a differential system of Duffing type via Caputo-Hadamard approach. *Appl. Math. Inform. Sci.* **2022**, *11*, 341–352.
4. Kang, Q.; Huang, B.; Zhou, M. Dynamic behavior of artificial Hodgkin-Huxley neuron model subject to additive noise. *IEEE Trans. Cybern.* **2015**, *46*, 2083–2093. [CrossRef] [PubMed]
5. Lv, M. Model of electrical activity in a neuron under magnetic flow effect. *Nonlinear Dyn.* **2016**, *85*, 1479–1490. [CrossRef]
6. Xing, M. Bifurcations and excitability in the temperature-sensitive Morris-Lecar neuron. *Nonlinear Dyn.* **2020**, *100*, 2687–2698. [CrossRef]
7. Zhang, X.; Ma, F.; Dai, Z.; Wang, J.; Chen, L.; Ling, H.; Soltanian, M.R. Radionuclide transport in multi-scale fractured rocks: A review. *J. Hazard. Mater.* **2022**, *424*, 127550. [CrossRef]
8. Tian, J.; Hou, M.; Bian, H. Variable surrogate model-based particle swarm optimization for high-dimensional expensive problems. *Complex Intell. Syst.* **2022**. [CrossRef]
9. Song, J.; Mingotti, A.; Zhang, J.; Peretto, L.; Wen, H. Accurate Damping Factor and Frequency Estimation for Damped Real-Valued Sinusoidal Signals. *IEEE Trans. Instrum. Meas.* **2022**, *71*, 1–4. [CrossRef]
10. Li, Q.K.; Lin, H.; Tan, X.; Du, S. H^∞ Consensus for Multiagent-Based Supply Chain Systems Under Switching Topology and Uncertain Demands. *IEEE Trans. Syst. Man Cybern. Syst.* **2018**, *50*, 4905–4918. [CrossRef]
11. Li, X.; Sun, Y. Stock intelligent investment strategy based on support vector machine parameter optimization algorithm. *Neural Comput. Appl.* **2020**, *32*, 1765–1775. [CrossRef]
12. Li, X.; Sun, Y. Application of RBF neural network optimal segmentation algorithm in credit rating. *Neural Comput. Appl.* **2021**, *33*, 8227–8235. [CrossRef]
13. Bao, B.; Rong, K.; Li, H.; Li, K.; Hua, Z.; Zhang, X. Memristor-coupled logistic hyperchaotic map. *IEEE Trans. Circuits Syst. II Express Br.* **2021**, *68*, 2992–2996. [CrossRef]
14. Peng, Y.; He, S.; Sun, K. A higher dimensional chaotic map with discrete memristor. *AEU-Int. J. Electron. Commun.* **2021**, *129*, 153539. [CrossRef]
15. Peng, Y.; Sun, K.; Peng, D.; Ai, W. Dynamics of a higher dimensional fractional-order chaotic map. *Phys. A Stat. Mech. Its Appl.* **2019**, *525*, 96–107. [CrossRef]
16. Khennaoui, A.A.; Ouannas, A.; Momani, S.; Almatroud, A.A.; Al-Swalha, M.M.; Boulaaras, S.M.; Pham, V.T. Special fractional-order map and its realization. *Mathematics* **2022**, *10*, 4474. [CrossRef]
17. Kong, S.; Li, C.; He, S.; Lai, Q. A memristive map with coexisting chaos and hyperchaos. *Chin. Phys. B* **2021**, *30*, 10502. [CrossRef]
18. Zhang, L.P.; Wei, Z.C.; Jiang, H.B.; Lyu, W.P.; Bi, Q.S. Extremely hidden multistability in a class of a two dimensional maps with a cosine memristor. *Chin. Phys. B* **2022**, *31*, 100503. [CrossRef]
19. Wang, J.; Gu, Y.; Rong, K.; Xu, Q.; Zhang, X. Memristor-based lozi map with hidden hyperchaos. *Mathematics* **2022**, *10*, 3426. [CrossRef]
20. Hodgkin, A.L.; Huxley, A.F. A quantitative description of membrane current and its application to conduction and excitation in nerve. *J. Physiol.* **1952**, *117*, 500–544. [CrossRef]
21. Gu, H.G.; Pan, B.B.; Chen, G.R.; Duan, L.X. Biological experimental demonstration of bifurcations from bursting to spiking predicted by theoretical models. *Nonlinear Dyn.* **2014**, *78*, 391–407. [CrossRef]
22. Chay, T.R. Chaos in a three-variable model of an excitable cell. *Phys. D* **1985**, *16*, 233–242. [CrossRef]
23. De, S.; Balakrishman, J. Brust mechanisms and brust synchronization in a system of coupled type-I and type neurons. *Commun. Nonlinear Sci. Number. Simul.* **2020**, *90*, 105391. [CrossRef]
24. Ouannas, A.; Batiha, I.M.; Pham, V.-T. *Fractional Discrete Chaos: Theories, Methods and Applications*; World Scientific: Singapore, 2023. [CrossRef]

25. Hioual, A.; Oussaeif, T.-E.; Ouannas, A.; Grassi, G.; Batiha, I.M.; Momani, S. New results for the stability of fractional-order discrete-time neural networks. *Alex. Eng. J.* **2022**, *61*, 10359–10369. [CrossRef]

26. Hioual, A.; Ouannas, A.; Oussaeif, T.-E.; Grassi, G.; Batiha, I.M.; Momani, S. On Variable-Order Fractional Discrete Neural Networks: Solvability and Stability. *Fractal Fract.* **2022**, *6*, 119. [CrossRef]

27. Li, Z.; Guo, Z.; Wang, M.; Ma, M. Firing activities induced by memristive autapse in Fitzhugh-nagumo neuron with time delay. *AEU Int. J. Electron. Commun.* **2021**, *142*, 153995. [CrossRef]

28. Bao, B.; Yang, Q.; Zhu, L.; Bao, H.; Xu, Q.; Yu, Y.; Chen, M. Chaotic bursting dynamics and coexisting multistable firing patterns in 3D autonomous Morris?Lecar model and microcontroller-based validations. *Int. J. Bifurc. Chaos* **2019**, *29*, 1950134. [CrossRef]

29. Ma, J.; Song, X.; Jin, W.; Wang, C. Autapse-induced synchronization in a coupled neuronal network. *Chaos Solitons Fract.* **2015**, *80*, 31–38. [CrossRef]

30. Qu, L.; Du, L.; Zhang, H.; Cao, Z.; Deng, Z. Regulation of chemical autapse on an FHN-ML neuronal system. *Int. J. Bifurcat. Chaos* **2019**, *29*, 1950202. [CrossRef]

31. Muni, S.S.; Rajagopal, K.; Karthikeyan, A.; Arun, S. Discrete hybrid Izhikevich neuron model: Nodal and network behaviours considering electromagnetic flux coupling. *Chaos, Solitons Fractals* **2022**, *155*, 111759. [CrossRef]

32. Hussain, I.; Jafari, S.; Perc, M.; Ghosh, D. Chimera states in a multi-weighted neuronal network. *Phys. Lett. A* **2022**, *424*, 127847. [CrossRef]

33. Li, C.; Yang, Y.; Yang, X.; Lu, Y. Application of discrete memristors in logistic map and Hindmarsh–Rose neuron. *Eur. Phys. J. Spec. Top.* **2022**, *231*, 3209–3224. [CrossRef]

34. Zhu, M.; Wang, C.; Deng, Q.; Hong, Q. Locally active memristor with three coexisting pinched hysteresis loops and its emulator circuit. *Int. J. Bifurcat. Chaos* **2020**, *30*, 2050184. [CrossRef]

35. Lin, H.; Wang, C.; Hong, Q.; Sun, Y. A multi-stable memristor and its application in a neural network. *IEEE Trans. Circuits Syst. Express Briefs* **2020**, *67*, 3472–3476. [CrossRef]

36. Adhikari, S.P.; Sah, M.P.; Kim, H.; Chua, L.O. Thre fingerprints of memristor. *IEEE Trans. Circuits Syst. I Regul. Pap.* **2013**, *60*, 3008–3021. [CrossRef]

37. Weither, M.; Herzig, M.; Tetzlaff, R.; Ascoli, A.; Mikolajick, T.; Sleazeck, S. Pattern formation with locally active S-type NbO_x mamristor. *IEEE Trans. Circuits Syst. I Reg. Pap.* **2019**, *66*, 2627–2638. [CrossRef]

38. Chen, M.; Sun, M.; Bao, H.; Hu, Y.; Bao, B. Fluc charge analysis of two-memristor- based Chua's circuit: Dimensionality decreasing model for detecting extreme multistability. *IEEE Trans. Ind. Electron.* **2019**, *67*, 2197–2206. [CrossRef]

39. Ma, M.; Lu, Y.; Li, Z.; Sun, Y.; Wang, C. Multistability and Phase Synchronization of Rulkov Neurons Coupled with a Locally Active Discrete Memristor. *Fractal Fract.* **2023**, *7*, 82. [CrossRef]

40. Ma, M.; Xiong, K.; Li, Z.; Sun, Y. Dynamic Behavior Analysis and Synchronization of Memristor-Coupled Heterogeneous Discrete Neural Networks. *Mathematics* **2023**, *11*, 375. [CrossRef]

41. Njitacke, Z.T.; Kengne, J. Complex dynamics of a 4D Hopfield neural networks (HNNs) with a nonlinear synaptic weight: Coexistence of multiple attractors and remerging Feigenbaum trees. *AEU—Int. J. Electron. Commun.* **2018**, *93*, 242–252. [CrossRef]